Journal of Sound and Vibration (2000) **229**(4), 913–933
doi:10.1006/jsvi.1999.2521, available online at http://www.idealibrary.com on IDEAL®

PERFORMANCE OF PENDULUM ABSORBER FOR A NON-LINEAR SYSTEM OF VARYING ORIENTATION

A. Ertas, O. Cuvalci and S. Ekwaro-Osire

Department of Mechanical Engineering, Texas Tech University, Lubbock, TX 79409, *U.S.A.*

(*Received* 11 *January* 1999, *and in final form* 22 *July* 1999)

Pendulum-type vibration absorbers are used extensively in engineering. These devices are particularly useful in practical applications where oscillations of a structure are to be constrained within a prescribed envelope. In this study, the primary structure under investigation consists of a flexible beam with a tip mass. The primary structure has a single degree of freedom and is subjected to vertical sinusoidal excitation at its base. Non-linearity in the primary structure is due to large deflections. The rotation point of the pendulum-type absorber is connected to the primary structure's tip mass. Together, the primary structure and absorber constitute a coupled system with two degrees of freedom. The motivation for study was the need to understand the effectiveness of passive vibration absorbers on structures that change their orientation, e.g., satellites. The primary objective is to assess the effectiveness of pendulum-type passive vibration absorber attached to a primary structure whose orientation varies. The orientations are at five degree increments about a vertical plane. In this study the orientation at which the absorber is effective is established and the factors that affect performance of the absorber are highlighted.

1. INTRODUCTION

Large flexible structures and aerospace structures can be studied by building a model consisting of flexible beams or columns with appendages. Since the oscillations of such structures are of large amplitude, this often can cause structural failure. In order to protect these structures from failure, suitable absorber devices are often installed to control or limit the amplitude of oscillation. Vibration absorbers have found extensive use in engineering. The recent activities in the area of design, development, and application of tuned vibration absorbers was provided by Sun *et al.* [1]. Korenev and Reznikov [2] offered an excellent collection of examples and consequent practical industrial application of such devices.

The underlying physical phenomenon of vibration attenuation involves energy transfer from a primary structure to a vibration absorber. This phenomenon can easily be demonstrated for quadratically non-linear systems that have autoparametric resonance [3]. For such systems, energy transfer may occur when the lower mode frequency is equal to one-half of the higher mode response may exponentially increase while the higher mode response may decrease due to the

0022-460X/00/040913 + 21 $35.00/0

energy transfer between the modes. Nayfeh and Mook [4] performed an extensive study on the energy transfer from low- to high-frequency modes. They showed the influence of internal resonance on this energy transfer. They also alluded to a situation were exciting a high-frequency mode resulted into large-amplitude oscillation in a low-frequency mode due to autoparametric resonance. Autoparametric resonance is one of the interesting research topics in vibration and has been studied extensively in literature [5–7]. Currently, in engineering, the most widely used passive absorbers include: tuned mass absorbers, impact absorbers, pendulum-type absorbers, beam absorbers, and last but not least, liquid absorbers. The response characteristics and effectiveness of which is well documented.

In most industrial application, vibration absorbers interact with non-linear structures. For this matter, the majority of analysis of vibration absorbers involves an excursion in non-linear dynamics. Assuming no damping, Arnold [8] investigated the steady state response of a primary structure with a non-linear dynamic vibration absorber. Using the Ritz averaging method, the author was able to approximately quantify the dynamics of the primary structure and non-linear absorber. Considering damping, Shaw *et al.* [9] carried out an extensive study on the behavior of a weakly non-linear vibration absorber. These researchers clearly demonstrated the occurrence of a combination resonance that was detrimental to the effectiveness of the absorber. An experimental and theoretical study of a pendulum absorber of a non-linear structure was conducted by Cuvalci and Ertas [10]. Tondl [11] demonstrated the effectiveness of an "inverted" pendulum-type absorber compared to the "traditional" pendulum absorber. It was clearly shown that the location of the oscillation point vis-à-vis the center of gravity did impact the effectiveness of the absorber.

2. DELAYED CO-ORDINATES

In the non-linear dynamics of systems, a two-dimensional phase space often used is the Torus. The most important long-term behavior derived behavior derived form a torus is quasiperiodicity. A concise experimental and theoretical overview on quasiperiodicity was presented by Glazier and Libchaber [12]. The theory proposed by the authors is effective only in the neighborhood of the transition to chaos. Mustafa and Ertas [13] presented experimental evidence of quasiperiodicity in a column-pendulum oscillator. Further, the same authors studied the detailed dynamics and bifurcation of a coupled oscillator [14].

The observation of the experimental model is the most challenging aspect in experimental dynamics. Experimental models generally have high-dimensional phase spaces, and the dimensions of the experimental model are far greater than the number of variables that can be measured. In this study, the mechanical system investigated was actually four dimensional. However, it was only possible to measure two displacement variables at a particular point to determine the actual dynamics of the system. The two variables measured, in this study, were the translational displacement of the primary structure and the angular displacement of the absorber. For a detailed analysis of the two experimentally extracted time

series, in terms of dynamical systems theory, state-space reconstruction had to be carried out. The method used in this study was based on Casdagli *et al.* [15] and it is briefly outlined below.

Consider a dynamical system whose response is governed by

$$\dot{x} = g(t, x) \tag{1}$$

and let its experimental reconstruction be sought. A quantity that is typically used for the values of state-space co-ordinate is the time series, $\{x(t_i)\}, i = 1, 2, \ldots, N$ and is obtained by sampling a co-ordinate of equation (1). Let $g: R \times M \to M$, with $\dim(M) = d$. The time series $x(t)$ is L-dimensional, $L < d$ and L is implicitly assumed one. Assuming that h is a measurement function $h: M \to R^{L=1}$, then a scalar time series can be formulated as

$$\zeta(t) = h(x(t)). \tag{2}$$

From the onset, the functions g and h are unknown. This state space is useful for qualitative analysis, such as phase portraits. For any measurable quantity with a well-selected time delay, vectors of the form of equation (2) can be constructed. Assuming a delay reconstruction map, which maps the states of a d-dimensional dynamical system into m-dimensional delay vectors

$$\Phi(x) = \{h(x), h(\phi_1(x)), \ldots, h(\phi_{2n}(x))\}, \tag{3}$$

where ϕ_t is the flow generated by the vector field g. Takens [16] showed that Φ is an embedding, where an embedding was defined as a smooth one-to-one transformation with a smooth inverse. Since Φ is an embedding, then there is a smooth dynamic G on the space of reconstructed vectors, i.e.,

$$G(\Phi(x)) = \Phi(g(x)), \tag{4}$$

where G is equivalent to the original dynamics g. The function G can be used for any purpose in the original dynamics. In reconstruction dynamics, the choice of the delay time τ is paramount. Ideally, the delay time is selected such that its value is neither too large nor too small. Mustafa and Ertas [13] provide a detailed discussion on the implications of the choice of a delay time.

As previously discussed, in this study only two quantities could be acquired from the experimental model, namely, the primary structure displacement $r_1(t)$ and the absorber angular displacement $r_2(t)$. The other two quantities sought, $r_1(t - \tau)$ and $r_2(t - \tau)$, were obtained using delay co-ordinate embedding. However, if any system was $N \geqslant 4$-dimensional, then according to Newhouse *et al.* [17], N could extend down to the case $N = 3$. If the system motion was assumed as quasiperiodic, one could seek the characteristics typical of a 3-torus. Based on the procedures outlined by Battelino *et al.* [18] and Mustafa and Ertas [13], a Poincaré section can be defined with two angles φ_1 and φ_2, such that

$$\varphi_1(i) = \arctan \frac{r_{1(t-\tau)}(i)}{r_{1(t)}(i)}, \quad \varphi_2(i) = \arctan \frac{r_{2(t-\tau)}(i)}{r_{2(t)}(i)}. \tag{5}$$

The Poincaré map, which is a 2-torus, can be defined by using the above angle definition such as

$$\varphi_1(i+1) = g_1(\varphi_1(i), \varphi_2(i)), \quad \varphi_2(i+1) = g_2(\varphi_1(i), \varphi_2(i)), \tag{6}$$

where g_1 and g_2 are experimentally extracted maps. One of the two angles above can be taken to be a constant thus reducing the dimension by one:

$$\varphi_1(i+1) = g_1(\varphi_1(i), \varphi_{2c}), \quad \varphi_2(i+1) = g_2(\varphi_{1c}, \varphi_2(i)), \tag{7}$$

where φ_{1c} and φ_{2c} are constant angles on the attractor. If the distribution of the points that lie on the one-dimensional attractor is smooth, the circle map is a one-to-one invertible map and any two locations from each equations (7) are topologically conjugate to a circle.

Based on the theoretical background provided in the previous sections, Mustafa and Ertas [14] used the afore outlined delay-co-ordinate embedding technique to investigate a flexible column with an appendage consisting of a mass-pendulum attached to its tip. And also Cuvalci and Ertas [10] studied the beam-tip mass-pendulum model as a vibration absorber device. The model was subjected to direct and parametric excitation. The dynamics of the primary structure was observed as a strong periodic motion because direct excitation was dominant on the system. The column-tip mass-pendulum model shows more complex behavior than the beam-tip mass-pendulum model because it was only subjected to parametric excitation. However, the experimental response curves show that the pendulum can

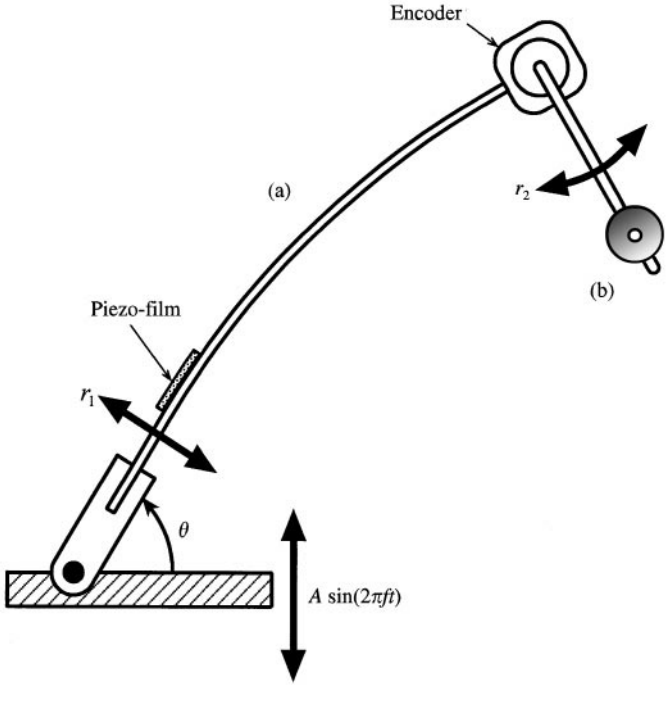

Figure 1. Mechanical model: (a) primary structure; (b) pendulum absorber.

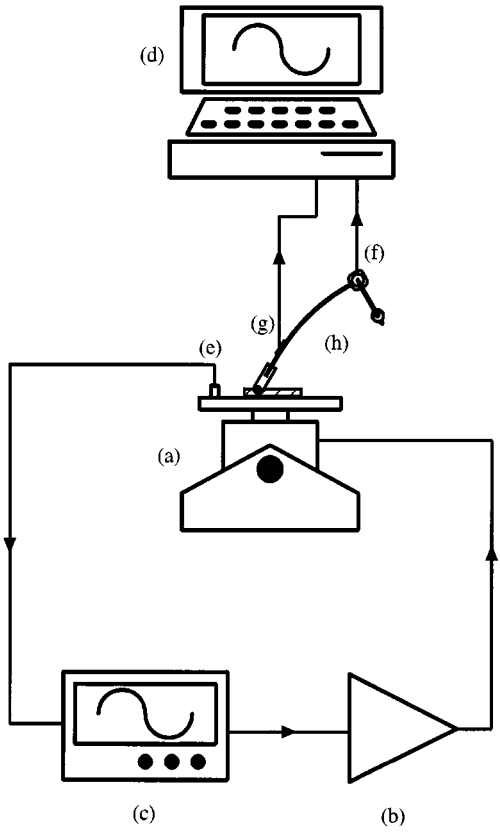

Figure 2. Experimental setup: (a) shaker table; (b) amplifier; (c) vibration control system; (d) acquisition and analysis; (c) accelerometer; (f) angle transducer; (g) displacement transducer; (h) mechanical model.

be used as a passive vibration absorber device for flexible structures. If such a system is rotated about a vertical xy-plane, does the absorber device still absorb energy from the primary structure? In this study, an attempt is made to answer the question. The motivation in answering the posed question results from the need of addressing the performance of passive absorbers attached to primary structures whose orientation changes, e.g., satellites. The objective of this study was to assess the effectiveness of a pendulum-type passive vibration absorber attached to a primary structure whose orientation varies. The orientation at which the absorber is effective was established and the factors that affect performance of the absorber were highlighted.

3. EXPERIMENTS

3.1. SETUP

The primary structure consisted of a slender beam (also referred to as "column" in upright position and as "beam" in horizontal position) of about 336 mm long

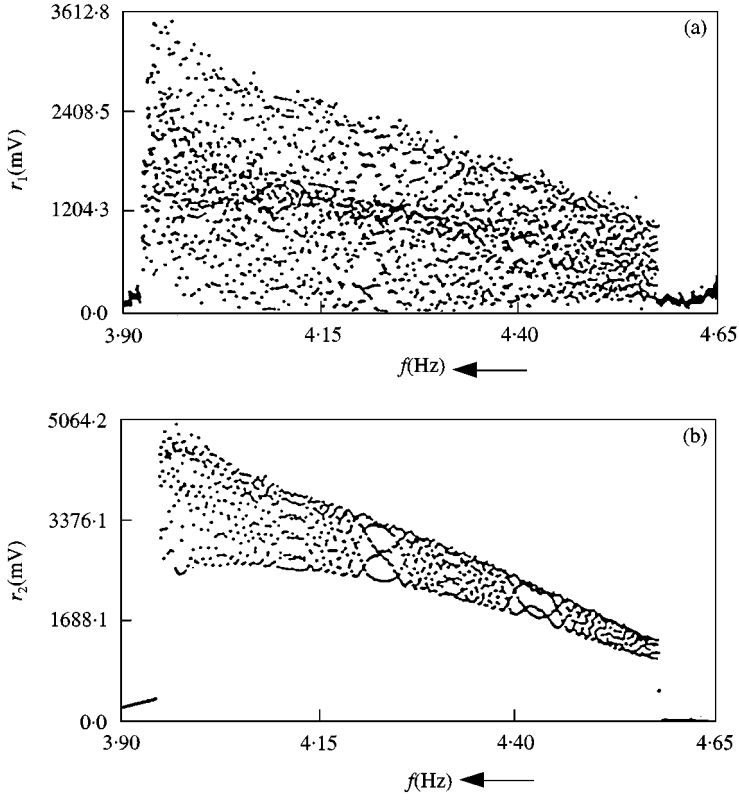

Figure 3. Response plots for the vertical orientation with $A = 300$ mV and 3·90 Hz $< f_o <$ 4·65 Hz: (a) primary structure; (b) absorber.

with a tip mass housing an encoder. The tip mass weighed about 212 g. The damping coefficient of the primary structure was determined to be about 0·07 kg s/m. The passive vibration absorber was of the pendulum-type consisting of a light composite rod with a mass at one end. The absorber is mounted on the primary structure to form the mechanical system shown in Figure 1. The primary structure is under sinusoidal excitation and undergoes large deflections. The equation of motion of such a coupled system is of the form

$$\dot{r}_1 = f_1(r_1, \dot{r}_1, r_2, \dot{r}_2) + \text{non-linear terms},$$
$$\dot{r}_2 = f_2(r_1, \dot{r}_1, r_2, \dot{r}_2) + \text{non-linear terms}, \quad (8)$$

where the non-linear terms are due to large deflections of the primary structure and the coupling between the primary structure and absorber.

The experimental set-up used in this study is shown in Figure 2. The setup consists of a shaker table (MB Dynamics C10E), amplifier (MB Dynamics S6K), vibration control system, acquisition and analysis, and transducers. In the latter setup, the vibration control was made up of sweep generator (Trig-Tek 701 LM), signal compressor (Trig-Tek 801 B), vibration monitor (Trig-Tek 610 B), and

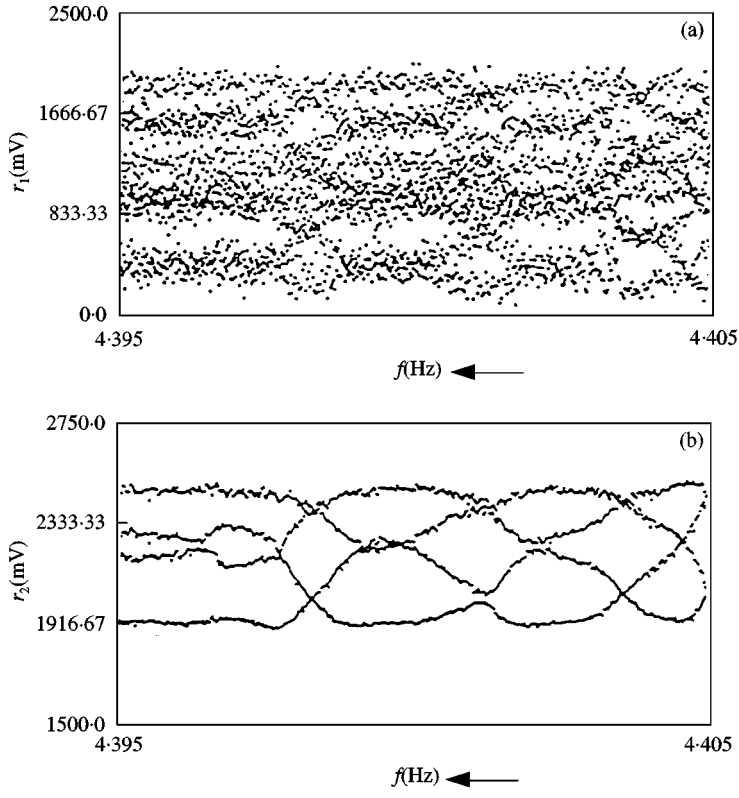

Figure 4. Response plot for the vertical orientation with $A = 300$ mV and 4·395 Hz $< f_o <$ 4·40 Hz: (a) primary structure; (b) absorber.

multi-level programmer (Trig-Tek 831). And the acquisition and analysis was made up of a computer (Apple Macintosh IIfx), boards (National Instruments NB-MIO-16X), software (National Instruments LabView 3.1), and signal analyzer (Model Data 600 4-channel). The transducers used were an accelerometer (PCB 353B52), a angle transducer (a in-house Opto-Digital-Encoder), and last but not least, a displacement transducer (piezo-film).

The shaker was mounted in the vertical direction and sinusoidal excitation was applied to the model. The excitation amplitude, excitation frequency, frequency increment and frequency range were programmed by using the vibration control system. The excitation frequency was incrementally varied between the upper and lower limits of the frequency range during the experimental period, or, if necessary, the excitation frequency was held constant. To measure the relative angular motion between the tip mass and the pendulum from the vertical downward position, an in-house opto-digital encoder, which was part of an angular measurement system, was used [19]. The encoder was housed in the tip mass at the end of the flexible beam (Figure 1). A piezo-film was used to measure the response of the flexible beam. An accelerometer sent a feedback signal to the vibration control system in order to control the output of the shaker. During the experiments, the excitation frequency,

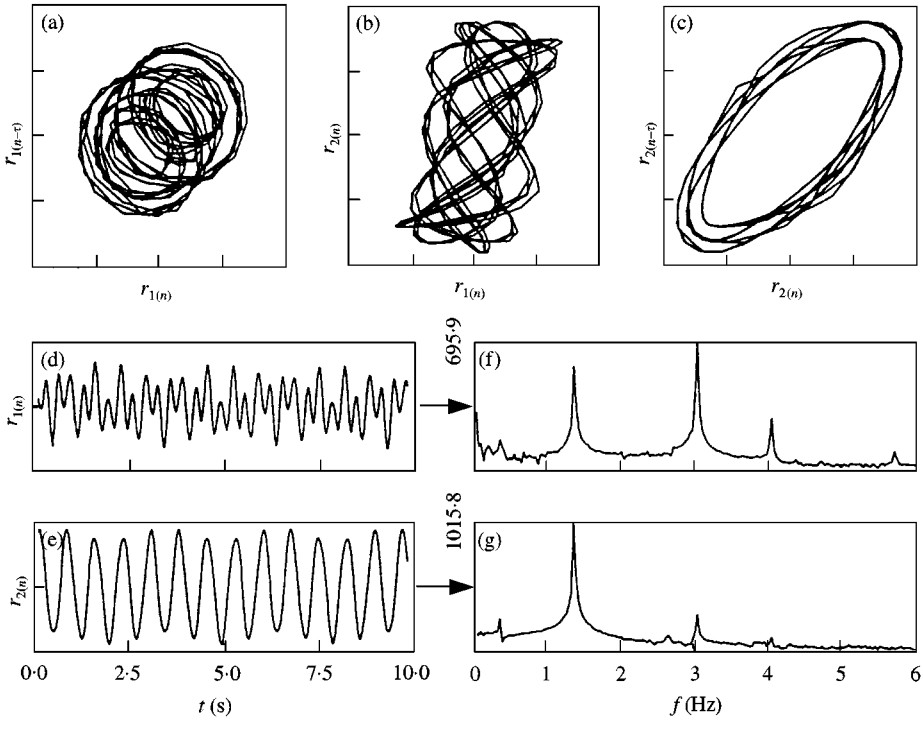

Figure 5. Response characteristics for the vertical orientation with $A = 300$ mV and $f_o = 4{\cdot}40$ Hz. Delay co-ordinates: (a) primary structures; (c) absorber; (b) projection on r_1–r_2 plane. Time history: (d) primary structure; (e) absorber. FFT: (f) primary structure; (g) absorber.

natural frequencies, excitation signal, and the Fast Fourier Transforms (FFT) of the response were observed through the signal analyzer. The Macintosh IIfx computer was used to store data from two channels, one was the piezo-film transducer to investigate the dynamics of the beam, and the other was the opto-digital-encoder to investigate the dynamics of the absorber. Additionally, the data analysis was done using the software LabView.

3.2. DATA ANALYSIS

To observe the dynamics of the experimental system, four categories of plots were extracted from experimental data. These included: frequency response curves, time histories, phase planes, FFT; cover of the 2-Torus, specified section on it, first return-map of specified section; and last but not least vibration absorption studies.

The first category of plots was frequency response curves. These plots include data obtained by sweeping between two frequencies. The latter sweep directions established after a series of experiments showed that indeed these directions did provide interesting responses of the system. The excitation amplitude was held constant during the sweep with the smallest sweep rate (0·1 oct/min), which was

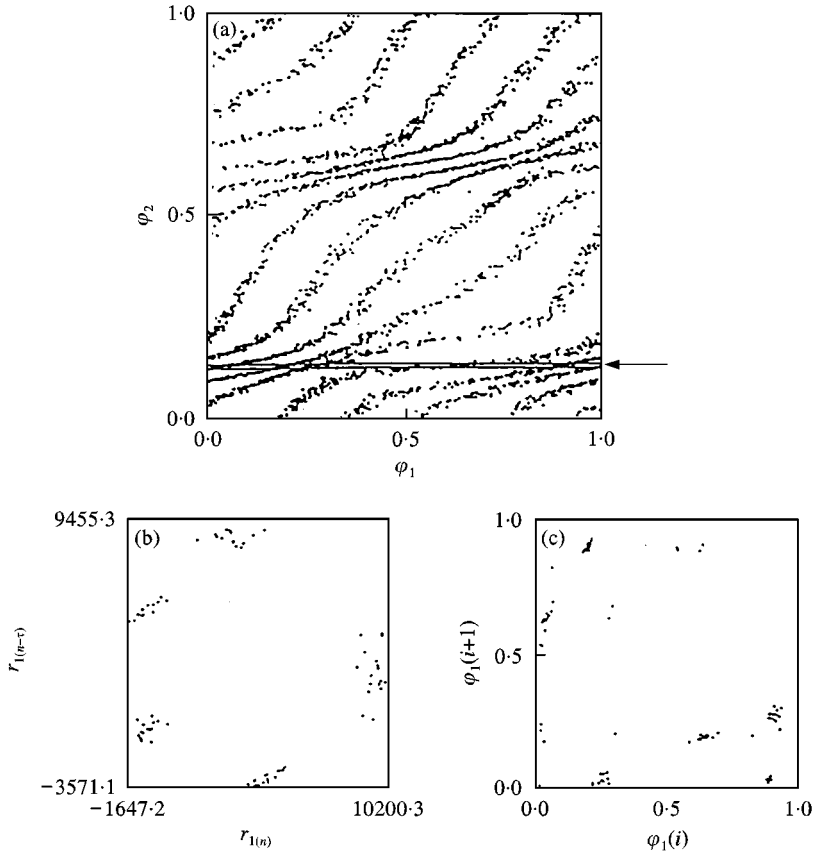

Figure 6. (5.11)-Periodic motion on T^2 for the vertical orientation with A = mV and f_o = 4·40 Hz: (a) cover of T^2; (b) slice of T^2; (c) first return map.

available from the vibration control system. The sweep rate was assumed small enough to reach the system steady state within each increment of forcing frequency. During the frequency sweep, special attention was paid to the nature of oscillations of the absorber. At the start of the down sweep the absorber showed no oscillation (first steady state). As soon as the absorber showed the first sudden increase in oscillations (first jump phenomenon), the sweep was halted at a constant forcing frequency for about 3 min. When oscillations of the absorber were deemed constant (second steady state), the frequency down sweep was once again initiated. As the down sweep progressed, when the absorber showed signs of losing its steady state oscillation (second jump phenomenon) the sweep was again halted for about 3 min. At the constant forcing frequency, when the absorber oscillations were again deemed constant (third steady state), the down sweep was again re-initiated and continued till the end of the experiment run. In all, during the down sweep, the response of the absorber depicted two jump phenomena which will clearly be shown in the response plots discussed in the next section of the paper. For the experiments where an up sweep was used, the previously outlined procedure was

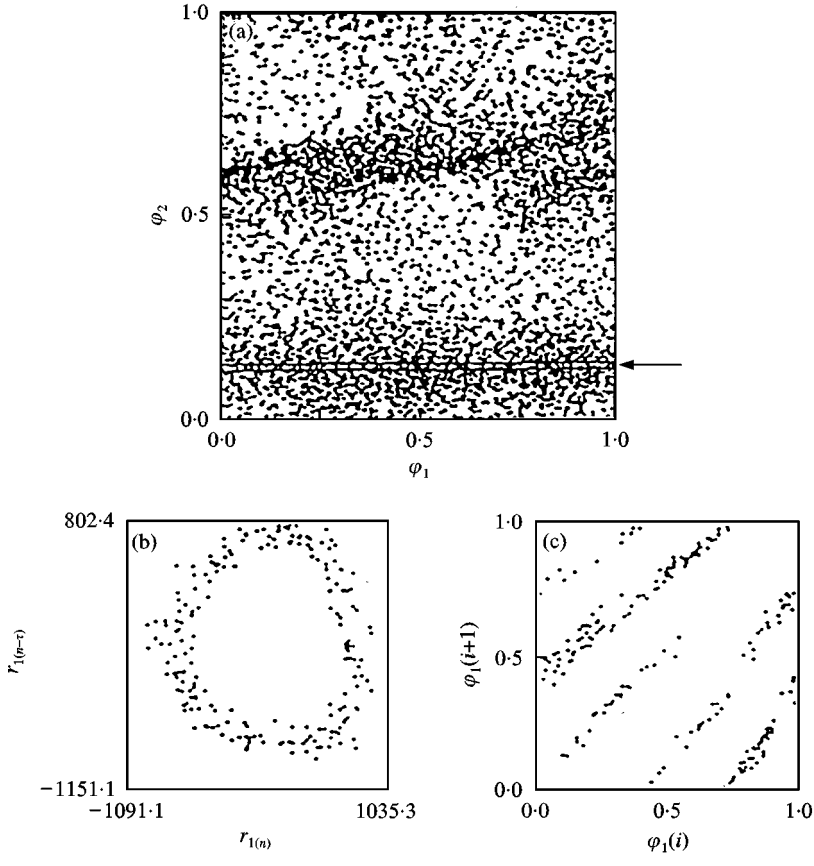

Figure 7. Quasiperiodic motion on T^2 for the vertical orientation with $A = 300$ mV and $f_o = 4{\cdot}37$ Hz: (a) cover of T^2; (b) slice of T^2; (c) first return map.

also followed. Experimental response curves were obtained by plotting local maximums of experimental data acquired during down sweep and up sweep.

The second category of plots includes time histories ($r_{1(n)}$ versus t and $r_{2(n)}$ versus t), phase planes ($r_{1(n-r)}$ versus $r_{1(n)}$, $r_{2(n-\tau)}$ versus $r_{2(n)}$, and $e_{2(n)}$ versus $r_{1(n)}$) and FFT. These plots were produced from time series that were recorded at constant forcing frequency and forcing amplitude by choosing a suitable delay time τ.

To further have an insight in the dynamics of the system, a third category of plots, pertaining to the torus, was justified. A torus is simply another two-dimensional phase space. This category of plots are based on equations (5)–(7). The plots show the cover of the 2-torus (φ_2 versus φ_1), specified section on it ($r_{1(n-\tau)}$ versus $r_{1(n)}$), and the first return map ($\varphi_1(i+1)$ versus $\varphi_1(i)$) of the specified section. If the response is periodic, there is a finite number of patterns on the cover of the 2-torus. We can say that the response is (n, m)-periodic, where n is the number to intersect φ_1-axis and m is the number to intersect φ_2-axis. A slice of the cover of a 2-torus can be taken parallel to the φ_1- or φ_2-axis. If the slice is taken parallel to the φ_1-axis, then the slice shows n discrete clusters of points. If it is taken

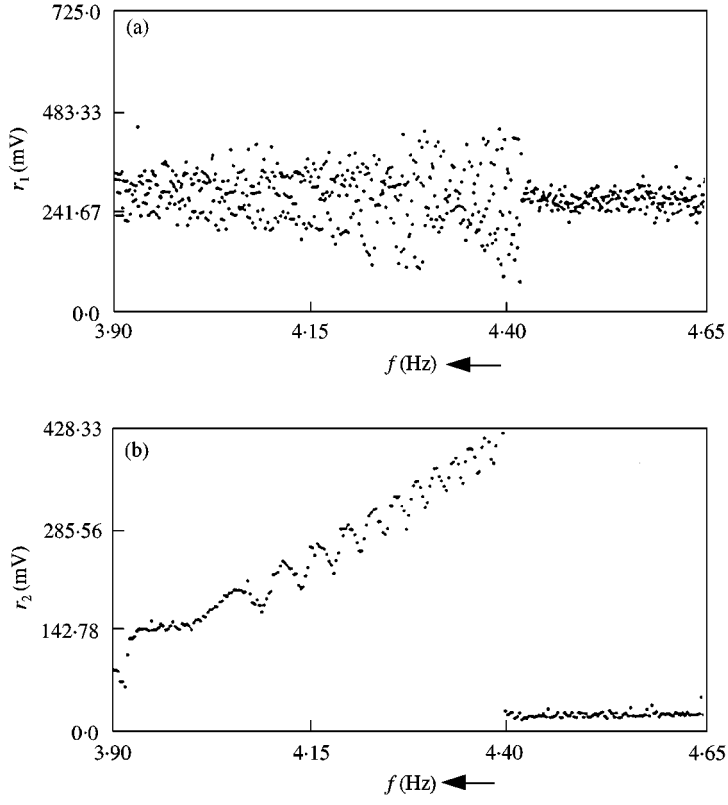

Figure 8. Response plots for $\theta = 25^\circ$ from vertical orientation with $A = 300$ mV and 3·90 Hz $< f_o <$ 4·65 Hz: (a) primary structure; (b) absorber.

parallel to the φ_2-axis, then m discrete clusters of points appear. The first return map was obtained from points lying on the slice by using $g_1^n(\varphi_1) = \varphi_1$ and $g_2^m(\varphi_2) = \varphi_2$ [cf. equation (7)]. If the response is qusiperiodic, the slice of the torus in both directions is a circle. The return map can be obtained in the same manner outlined above.

The fourth category of plots was vibration adsorption studies. The first plot in this category shows maximum displacements of the primary structure and the absorber, the response relation between the two modes and the absorption regions with respect to the rotating angle. To obtain the primary structure and the absorber maximum displacement plot at the selected forcing frequency, the maximum amplitude of the primary structure and the absorber were extracted from the steady state oscillation for every 5° angle and marked on the plot. The response relation plots were obtained by observing the dynamics relation between the system and the absorber (one-to-two or one-to-one). To obtain the last plot in this group, experiments were performed in the selected forcing frequency range for up and down sweeps at different forcing amplitudes and rotating angles. During the sweeps, the frequencies at which the absorber started and ended oscillating were observed and the region between the two frequencies was defined as *absorption region.*

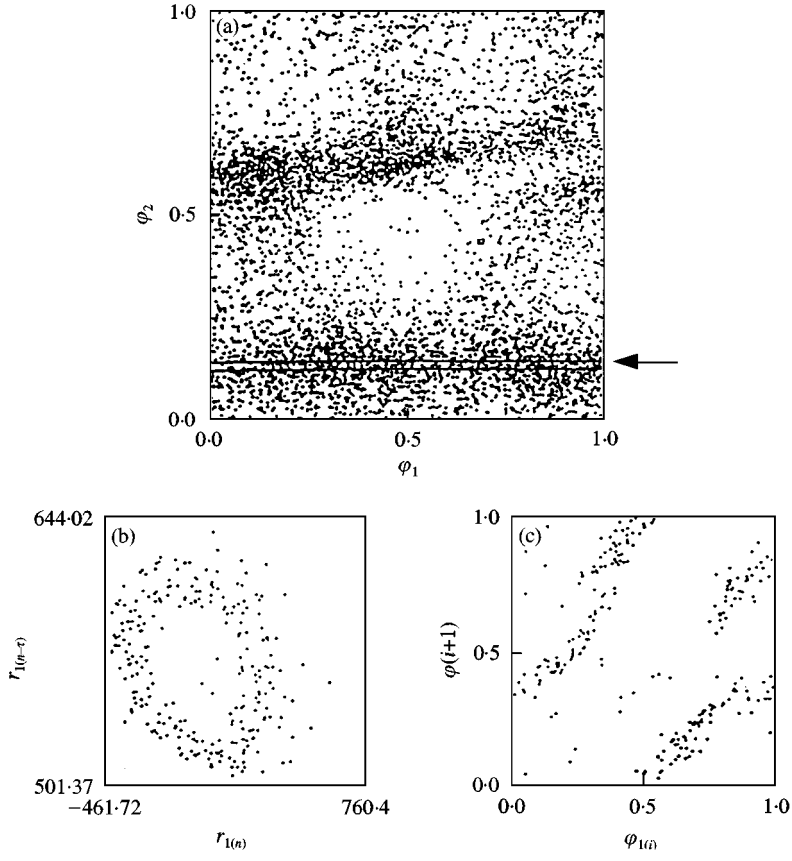

Figure 9. Quasiperiodic motion on T^2 for $\theta = 25^\circ$ from the vertical orientation with $A = 300$ mV ($f_o = 4{\cdot}25$ Hz): (a) cover of T^2; (b) slice of T^2; (c) first return map.

4. RESULTS AND DISCUSSIONS

Experimental investigations were conducted to obtain the frequency response curves for a range of excitation frequencies, which included the natural frequency of the system. Phase planes, time histories, FFT, and first return map were also done to detail the dynamics of the system. In both the horizontal and vertical orientations, the natural frequencies of the system and absorber were tuned to $f_s = 2{\cdot}80$ Hz and $f_a = 1{\cdot}40$ Hz respectively. During the experiments, the natural frequency of the system, the tip mass, the pendulum mass, and the internal frequency ratio were not altered. In order to obtain the system dynamics the experiments were conducted starting from the horizontal position (beam) to the

Figure 11. Response characteristics for the horizontal orientation with $A = 300$ mV and $f_o = 3{\cdot}00$ Hz. Delay co-ordinates: (a) primary structures; (c) absorber; (b) projection on r_1–r_2 plane. Time history: (d) primary structure; (e) absorber. FFT: (f) primary structure; (g) absorber.

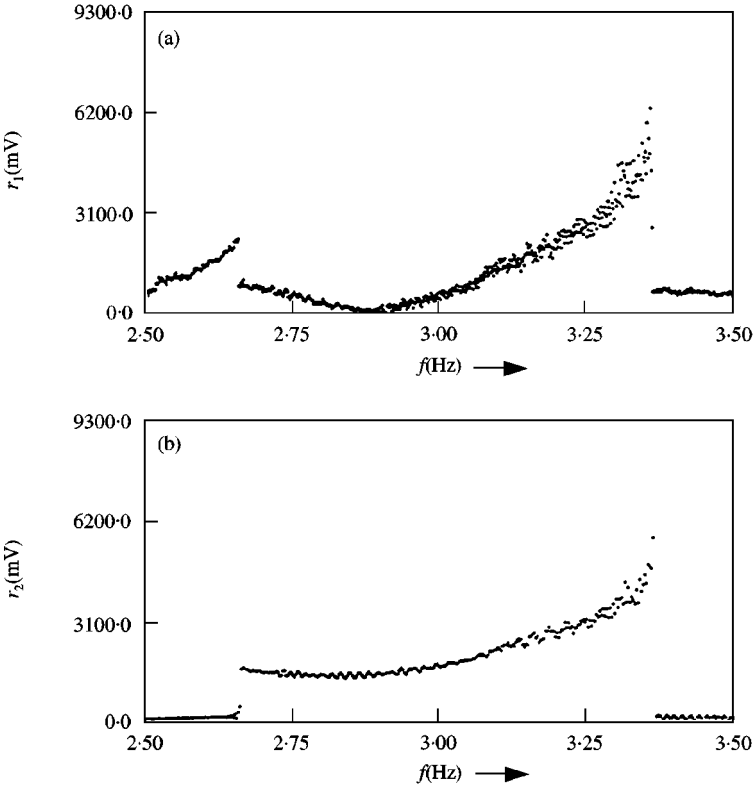

Figure 10. Response plots for the horizontal orientation with $A = 300$ mV and $2{\cdot}50\ \text{Hz} < f_o < 3{\cdot}50\ \text{Hz}$: (a) primary structure; (b) absorber.

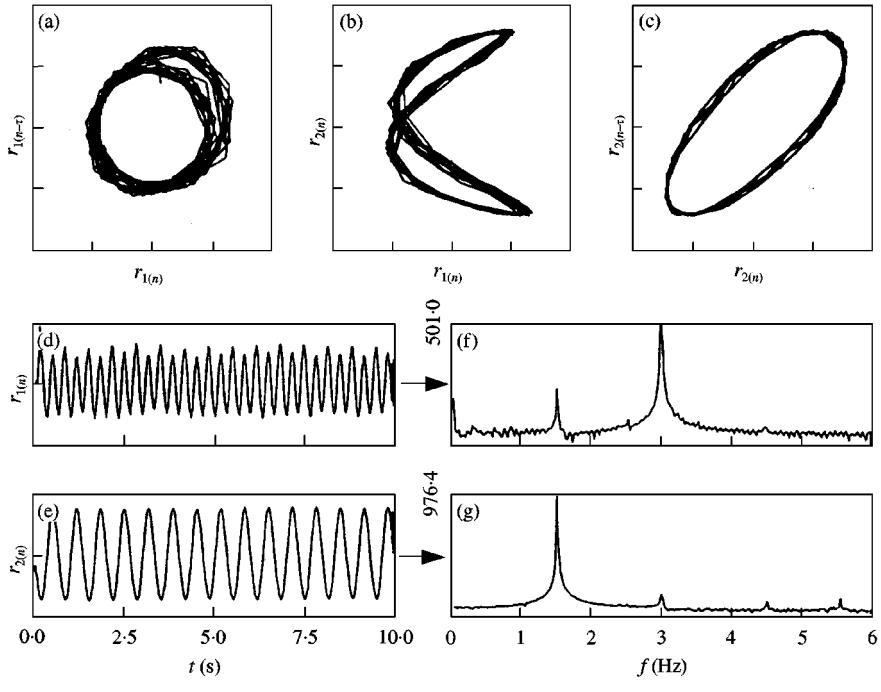

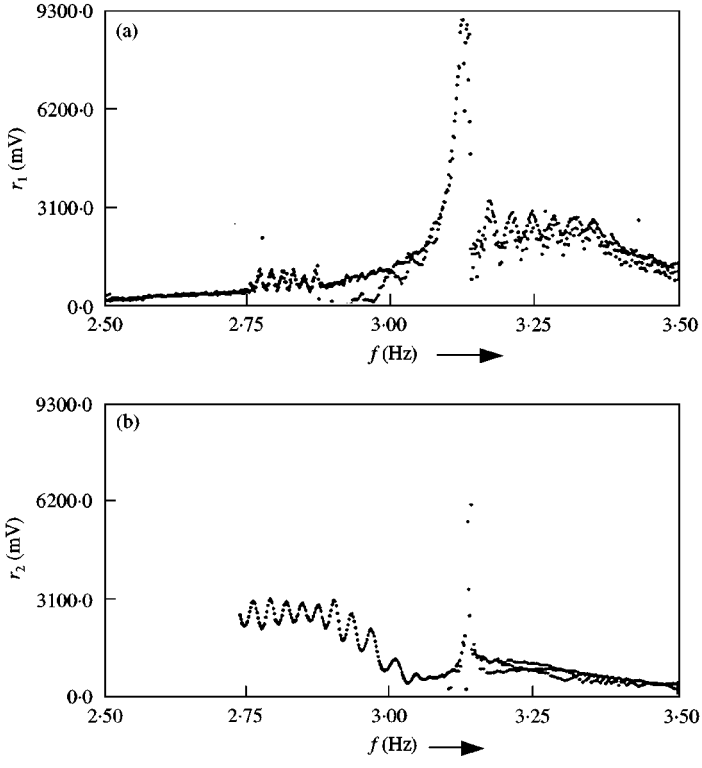

Figure 12. Response plots for $\theta = 70^\circ$ from horizontal orientation with $A = 300$ mV and 2·50 Hz $< f_o <$ 3·50 Hz: (a) primary structure; (b) absorber.

vertical position (column) with 19 different angles and vice versa. For the experiments starting from the horizontal position to vertical position, the excitation frequency was swept *up*, from 2·50 to 3·50 Hz. This frequency range spanned $f_s = 2f_a = 2{\cdot}80$ Hz. For the experiments starting from the vertical position to horizontal position, the excitation frequency was swept *down*, from 4·65 to 3·90 Hz. This frequency range spanned $1{\cdot}5f_s = 3f_a = 4{\cdot}20$ Hz.

Experiments were performed for two main setups. First, the model was set-up as a beam-tip mass-pendulum system. Then it was rotated in 5° increments to the vertical orientation. Second, the model was set-up as a column-tip mass-pendulum system. Then it was rotated in 5° increments to the horizontal orientation. For both cases, the internal frequency ratio was tuned in the initial position (vertical or horizontal) of the system, such as $f = f_s = 2f_a$. The above ratio remained unchanged for each of the rotation. To investigate the system response, the excitation frequency was swept down or up about a selected interval at the sweep rate of 0·1 oct/min with a constant amplitude.

Figure 3 shows the response plots for the vertical orientation for an excitation amplitude of $A = 300$ mV. The excitation frequency was swept down from 4·65 to 3·90 Hz. Note that in the response plots, of this study, the direction of the sweep is indicated by the arrow in the label of the abscissa. The response of the primary structure and absorber show a response jump at 3·95 and 4·58 Hz. The absorber

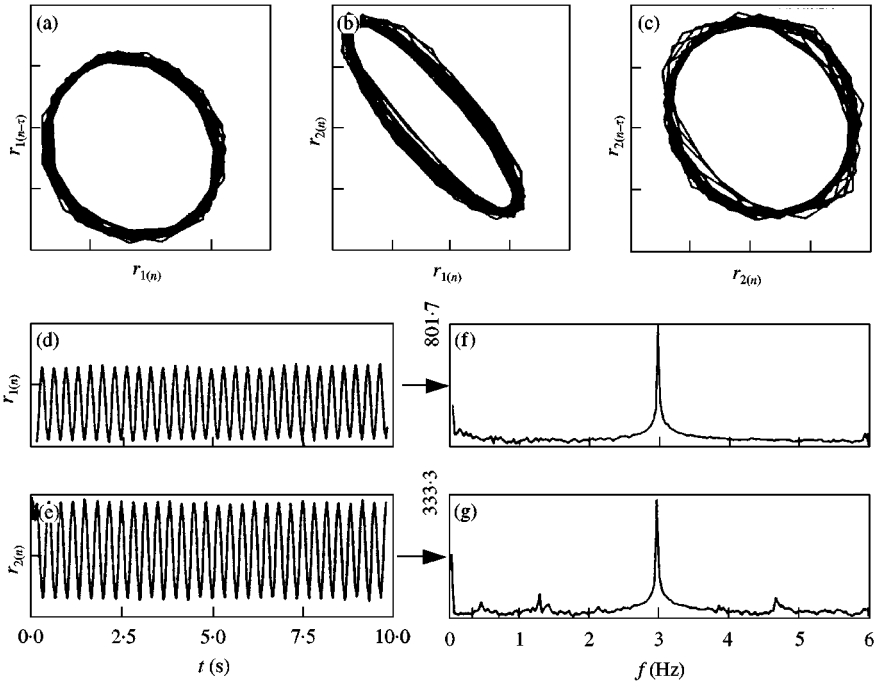

Figure 13. Response characteristics for $\theta = 70^\circ$ from horizontal orientation with $A = 300$ mV and $f_o = 2{\cdot}95$ Hz. Delay co-ordinates: (a) primary structures; (c) absorber; (b) projection on r_1–r_2 plane. Time history: (d) primary structure; (e) absorber. FFT: (f) primary structure; (g) absorber.

response is quasiperiodic with widows of periodicity. This observation is akin to that made by other researchers [13]. To analyze the motion, experiments were performed for smaller ranges of the chosen interval. Figure 4 shows the response of the primary structure and absorber for a smaller frequency range of $f_o \in (4{\cdot}395, 4{\cdot}405)$. From this figure the absorber response is clearly periodic. The primary structure also depicts some periodicity, though there were some scatters in the response, possibly related to the piezo-film instead of the dynamics of the structure.

To further analyze the dynamics of the absorber and primary structure, the response at the excitation frequency, $f_o = 4{\cdot}40$ Hz, was analyzed. Figure 5 show the reconstructed dynamics, time series, and FFT plots for the vertical orientation with $A = 300$ mV. In Figures 5(f) and 5(g), the signal was not filtered and shows the FFT for the primary structure and the absorber respectively. As seen from Figure 5(f) the primary structure has harmonics of $f \approx 3{\cdot}0$ Hz, related to the natural frequency of the primary structure, and $f \approx 1{\cdot}5$ Hz, which is related to the coupling effect. In Figure 5(g) the absorber has harmonics of $f \approx 1{\cdot}5$ Hz, related to the natural frequency of the absorber, and $f \approx 3{\cdot}0$ Hz, which is related to the coupling effect. The forcing frequency was $f_o \approx 4{\cdot}40$ Hz but could not be seen as a harmonic in Figures 5(f) and 5(g) because the parametric excitation was more dominant than the direct (or external) excitation. From Figure 5, it is clear that the response of both absorber and primary structure shows periodicity. In Figures 5(c) and 5(g) it is clear that the absorber shows periodicity with a dominant single frequency. On the

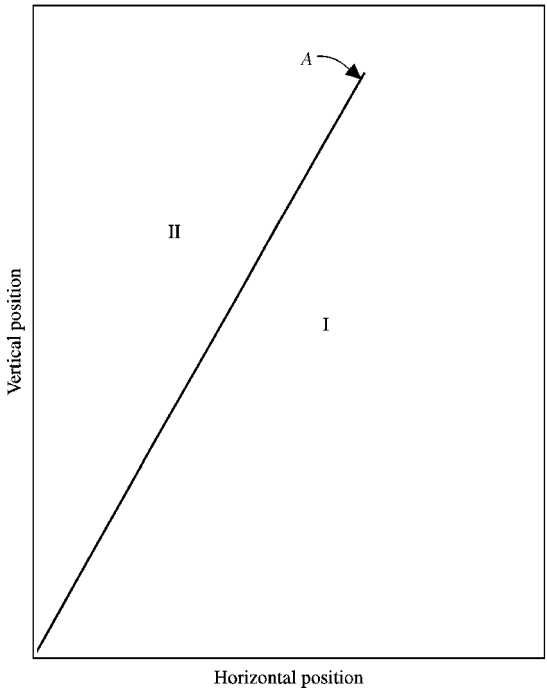

Figure 14. Critical boundary definition: A, critical boundary; I, absorption region (Region I); II, non-absorption region (Region II).

other hand, Figures 5(a) and 5(f), the primary structure response is also periodic but more frequencies are in play. To fully ascertain the periodicity, patterns on the torus were studied at the excitation amplitude of $A = 300$ mV and excitation frequency of $f_o = 4{\cdot}40$ Hz (Figure 6). A square with periodic boundary conditions is used to best depict the phase portraits [20]. A response is (m, n)-periodic if its orbits can be shown to intersect the θ_1 and θ_2-axis m and n times respectively. Based on the latter approach, it can be seen from Figure 6(a) that the response of the primary structure depicts a (5, 11)-periodic motion on T^2. Slices of the cover of T^2, Figures 6(b) and 6(c), confirm the (5, 11)-periodicity.

Again, referring to Figure 3, an excitation frequency of $f_o = 4{\cdot}37$ Hz is selected to investigate the possibility of the quasiperiodic motion (Figure 7). Figure 7(a) shows that the torus is dense with orbits. And additionally, the slice of the torus, Figure 7(b), shows that the orbit points form a closed path. The latter observations from Figure 7 confirm that the response is qusiperiodic.

Experiments of the system were conducted at orientations of 5° increments from the vertical orientation. Figure 8 shows the response plots at $\theta = 25°$ from the vertical orientation with $A = 300$ mV and the excitation frequency was swept down from 4·65 to 3·90 Hz. On comparing Figures 8 and 3, it is observed that the overall magnitude of the primary structure response amplitude in Figure 8 is less by a factor of 10 compared to that in Figure 3. From Figure 8, it is evident that the primary structure can hardly drive the absorber. At this orientation ($\theta = 25°$) the

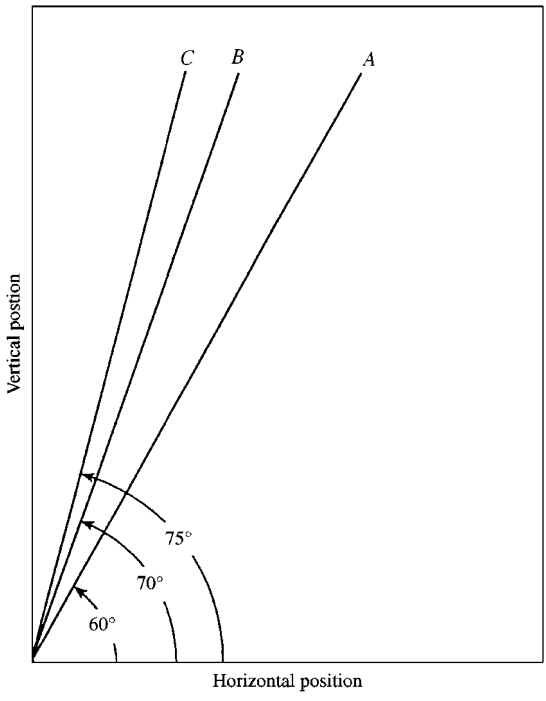

Figure 15. Critical boundaries (rotating from horizontal position) for $A = 100$, 300, 400 mV in curves A, B, C respectively.

detail dynamics were studied as $f_o = 4{\cdot}25$ Hz. (Figure 9). At this system orientation, quasiperiodicity was still evident.

The experimental response curve (Figure 10) shows for the system in the horizontal orientation for an excitation amplitude $A = 300$ mV. In this case, the excitation frequency was swept up from 2·50 to 3·50 Hz. This figure shows clear interaction between the absorber and primary structure. It is seen from this figure that as the frequency is swept up, the primary structure initially oscillates while the absorber hardly oscillates. But at about 2·65 Hz, an energy transfer occurs from the primary structure to the absorber. This is a similar trend observed by other authors [10] for a similar system. Detailed dynamics of the motion, for $f_o = 3{\cdot}00$ Hz, are shown in Figure 11. Based on Figures 11(g) and 11(f), it is evident that the dominant response frequency of the absorber ($\approx 1{\cdot}5$ Hz) is half the response frequency of the primary structure (≈ 3 Hz). It is important to note that the predominant oscillation frequency of the primary system is that of the direct (or external) excitation.

Experiments were conducted of the system at orientations of 5° increments from the horizontal orientation. Figure 12 shows the response plots at $\theta = 70°$ from the horizontal orientation with $A = 300$ mV and the excitation frequency was swept up from 2·50 to 3·50 Hz. At this orientation, the energy exchange between the absorber and primary structure is substantially weaker. For this orientation, detailed dynamics were conducted at an excitation frequency of $f_o = 2{\cdot}95$ Hz (Figure 13). At

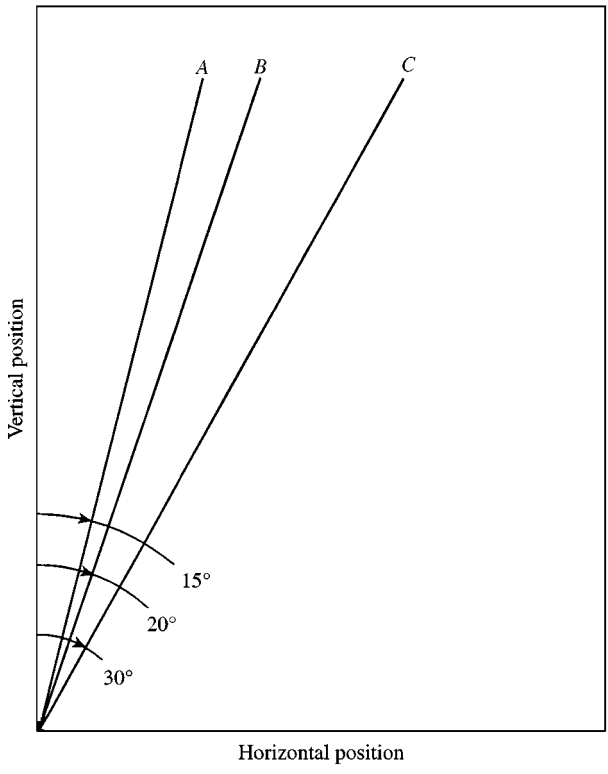

Figure 16. Critical boundaries (rotating from vertical position) for $A = 100, 300, 400$ mV in curves A, B, C respectively.

this excitation frequency both the primary system and absorber oscillate at the same frequency (≈ 3 Hz). This is the evidence of a one-to-one coupling. This observation implies that the autoparametric relation (one-to-two) between the primary structure and absorber has disappeared resulting in zero energy transfer between the primary structure and absorber. Hence, at this orientation, the absorber is ineffective.

A series of experiments were conducted at 5° increments from the vertical orientation and at 5° increments from the horizontal orientation. An orientation was established beyond which a one-to-one coupling was evident, or in other words, the absorber was ineffectual. This angle orientation is referred to as the *critical boundary*. Below the *critical boundary* an one-to-two ($f_o = f_s = 2f_a$) relation exists and the absorber is effective. The region where the absorber is effective will also be referred to as Region I. On the other hand, above the *critical boundary* an one-to-one ($f_o = f_s = f_a$) relation exists and the absorber is ineffective. The region where the absorber is ineffective will also be referred to as Region II. The *absorption region* studied here is the parametric resonance of the system. It should further be noted that this system does not dissipate energy, but rather energy is transferred from one mode to another. This is due to the fact that system under study is coupled.

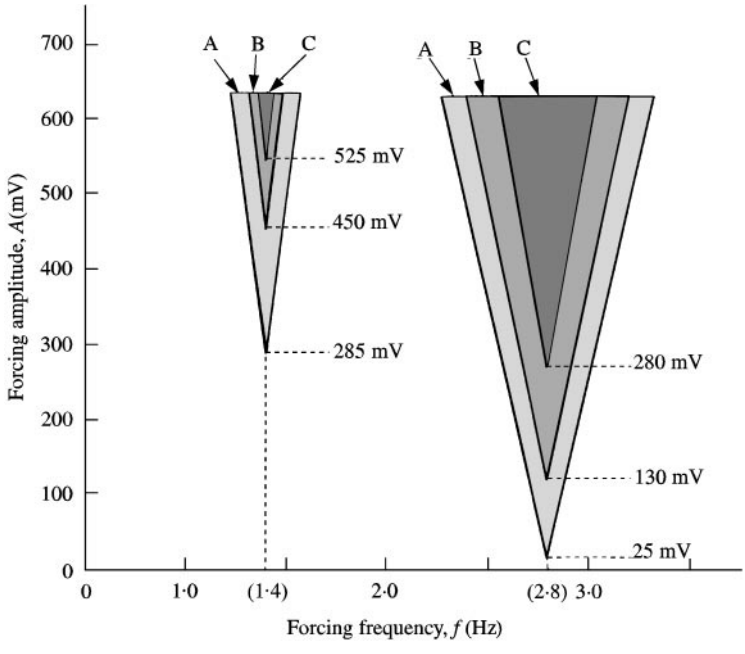

Figure 17. Absorption regions (rotating from horizontal position) for $\theta = 0, 45, 60^\circ$ in areas A, B, C respectively.

Figure 14 depicts the definition of a *critical boundary*, where to the right of the boundary is the Region I, and to the left is Region II. As will be shown later, the location of the two regions, relative to the *critical boundary* is dependent on whether the rotation is from the horizontal or vertical position. Figures 15 shows the effect of the excitation amplitude on the *critical boundary* measured from the horizontal orientation. For each of the three critical boundaries in Figure 15, Regions I and II are on the right side and left side respectively. From this figure, it is evident that increase of the excitation amplitude leads to an increase in the *absorption region* of the absorber. Figure 16 shows the effect of the excitation amplitude on the *absorption region* at an orientation measured from the vertical orientation. In this figure Region I is on the left side of each *critical boundary*. In Figure 16, an increase of the excitation amplitude also translates to an expansion of the *absorption region*, hence an increase of the angle of the *critical boundary*. It is observed that the critical boundaries *A*, *B*, and *C* in Figure 15 coincide with critical boundaries *C*, *B*, and *A* in Figure 16 respectively.

Figure 17 portrays the variation of the *absorption region* with respect to rotation angle and forcing amplitude. In this figure, only the orientation from the horizontal position was selected for analysis. In this case, the natural frequency of the system, f_s was 2·80 Hz. For this exhibit, the system was tuned such that the conditions $f_o = \frac{1}{2} f_s = f_a = 1{\cdot}4$ Hz and $f_o = f_s = 2f_a = 2{\cdot}8$ Hz were satisfied where the former is the subharmonic condition and the latter is the autoparametric resonance condition. As seen from this figure, the absorber absorbs energy from the primary structure,

even when the primary structure is subjected to a very small excitation amplitude ($A = 25$ mV) in the neighborhood of the autoparametric resonance ($f_o = f_s = 2f_a$). For the subharmonic resonance case, comparing to the fundamental resonance case a very small *absorption region* was observed related to the rotation angle at very high forcing amplitude. From Figure 17, increasing the rotation angle of orientation narrowed the *absorption region*. It can also be observed from this figure that with an increase in the rotation angle of orientation, required a higher excitation amplitude A for the absorber to begin oscillating.

5. CONCLUSIONS

Based on the narrative in the previous section, a number of conclusions can be drawn. First, the system in vertical direction shows more complex dynamics than the system in horizontal direction. Secondly, the energy is absorbed from the system by the absorber until a *critical boundary* is reached. The range of this *critical boundary* is shown to depend on the forcing amplitude, whereby increasing the forcing amplitude results in an increase of the boundary region. Thirdly, the systematic approach developed in this study can be used to establish the demarcation of the effectiveness of the passive vibration absorber for systems that change their orientation. This has practical implication since it has been shown that for primary structures that change orientation, passive vibration absorbers may become mistuned and consequently lose their effectiveness.

REFERENCES

1. J. Q. Sun, M. R. Jolly and M. A. Norris 1995 *Journal of Mechanical Design* **117**, 234–242. Passive, adaptive and active tuned vibration absorbers—a survey.
2. B. G. Korenev and L. M. Reznikov 1993 *Dynamic Vibration Absorbers*. New York: Wiley.
3. S. S. Oueini, A. H. Nayfeh and J. R. Pratt 1998 *Nonlinear Dynamics* **15**, 259–282. A nonlinear vibration absorber for flexible structures.
4. A. H. Nayfeh and D. T. Mook 1995 *Journal of Mechanical Design* **117**, 186–195. Energy transfer from high-frequency to low-frequency modes in structures.
5. B. McLaughlin 1981 *Journal of Statistical Physics* **24**, 375–388. Period-doubling bifurcation and chaotic motion for a parametrically forced pendulum.
6. H. Sprysl 1987 *Journal of Sound and Viburation* **112**, 63–67. Internal resonance of non-linear autonomous vibrating systems with two-degrees-of-freedom.
7. L. D. Zavodney and A. H. Nayfeh 1986 *International Journal of Non-Linear Mechanics* **24**, 105–125. The nonlinear response of a slender beam carrying a lumped mass to a principle parametric excitation: theory and experiment.
8. F. R. Arnold 1955 *Journal of Applied Mechanics* **22**, 487–492. Steady-state behavior of system provided with nonlinear dynamic vibration absorber.
9. J. Shaw, S. W. Shaw and A. G. Haddow 1989 *International Journal of Non-Linear Mechanics* **24**, 281–293. On the response of the non-linear vibration absorber.
10. O. Cuvalci and A. Ertas 1996 *Journal of Vibration and Acoustics* **118**, 558–566. Pendulum as vibration absorber for flexible structures: experiments and theory.
11. A. Tondl 1998 *Acta Technica CSAV* **43**, 301–309. Vibration quencing of an externally excited system by means of dynamic absorber.

12. J. A. Glazier and A. Libchaber 1998 *IEEE Transactions on Circuits and Systems* **35**, 790–806. Quasi-periodicity and dynamical systems: an experimental's view.
13. G. Mustafa and A. Ertas 1995 *Journal of Dynamic Systems, Measurement, and Control* **117**, 218–225. Experimental evidence of quasiperiodicity and its breakdown in the column-pendulum oscillator.
14. G. Mustafa and A. Ertas 1995 *Journal of Sound and Vibration* **182**, 393–413. Dynamics and bifurcations of a coupled column-pendulum oscillator.
15. M. Casdagli, S. Eubank, J. D. Farmer and J. Gibson 1991 *Physica D* **51**, 52–58. State space reconstruction in the presence of noise.
16. F. Takens 1981 *Dynamical Systems and Turbulence* (D. S. Rand and L.-S. Young, editors). New York: Springer-Verlag Detecting strange attractors in turbulence.
17. S. E. Newhouse, D. Ruelle and F. Takens 1978 *Communications in Mathematical Physics* **64**, 35–40. Occurrence of strange axiom A attractors near quasi periodic flow on T^m, $m \geqslant 3$.
18. P. M. Battelino, C. Grebogi, E. Ott and J. A. Yorke 1989 *Physica D* **39**, 299–314. Chaotic attractors on a 3-torus, and torus break-up.
19. A. Ertas and G. Mustafa 1992 *Experimental Techniques* **16**, 33–35. Real-time response of the simple pendulum: an experimental technique.
20. S. H. Strogatz 1994 *Nonlinear Dynamics and Chaos*. Reading, MA: Addsion-Wesley.

APPENDIX: PRINCIPAL NOTATION

A	forcing amplitude (peak-to-peak)
f	frequency (Hz)
f_a	natural frequency of absorber (Hz)
f_o	forcing frequency (Hz)
f_s	natural frequency of system (Hz)
r_1	translational displacement of primary structure
r_2	angular displacement of absorber
$r_{1(n-\tau)}$	delay co-ordinate of primary structure
$r_{2(n-\tau)}$	delay co-ordinate of absorber
T^2	two-dimensional torus (2-torus)
θ	variable angle from the horizontal position and the vertical position
τ	delay time
φ_1	angular co-ordinate of T^2 formed by $r_{1(t-\tau)}$ and $r_{1(i)}$ (primary structure)
φ_2	angular co-ordinate of T^2 formed by $r_{2(t-\tau)}$ and $r_{2(t)}$ (absorber)